THE JOURNAL OF PHYSICAL CHEMISTRY C

Article

pubs.acs.org/JPCC

Plasmon-Sampled Surface-Enhanced Raman Excitation Spectroscopy on Silver Immobilized Nanorod Assemblies and Optimization for Near Infrared (λ_{ex} = 1064 nm) Studies

Nathan G. Greeneltch, Martin G. Blaber, George C. Schatz,* and Richard. P. Van Duyne*

Supporting Information

ABSTRACT: For many Surface-Enhanced Raman Spectroscopy (SERS) applications, the enhancing substrate must exhibit a number of critical properties that include low cost, robustness, and reproducibly high enhancement over large areas of the substrate. In this study we investigate the SERS fundamental enhancement factor of silver Immobilized Nanorod Assembly (AgINRA) substrates as a function of both the dielectric sphere diameter (310−780 nm) and the input laser wavelength (633−1064 nm) with a technique called plasmon-sampled surface-enhanced Raman excitation spectroscopy (PS-SERES). The nonresonant molecule benzenethiol was chosen as the probe molecule. Higher enhancement factors (EFs) were measured as the plasmon resonance and excitation wavelength's relative separation were optimized and both moved toward the infrared region, ultimately eclipsing the 10^8 mark. This is the highest EF to date measured on this type of large-area substrate. The enhancement factors reported here are the result of efficient coupling between free space photons and the surface plasmon states in the metal INRA substrate. Coupled with their robustness and ease of fabrication, these results further underscore the value and versatility of metal INRA substrates in the field of surface-enhanced Raman spectroscopy.

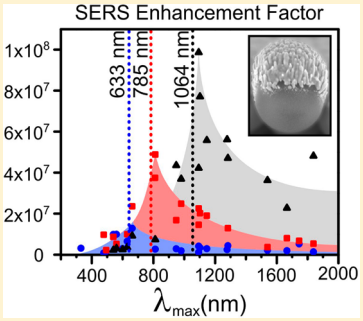

INTRODUCTION

Localized surface plasmon resonances (LSPRs) on noble metal nanostructures lead to strongly enhanced local electric fields.[1−4] This field localization can be used to enhance fluorescence,[5] luminescence,[6] photoabsorption,[7] and Raman scattering.[8,9] In surface-enhanced Raman spectroscopy (SERS), both the incident field and the field scattered by the molecule are enhanced.[2,3,10−12] This leads to a SERS intensity that scales like the surface average of the forth power of the normalized field ($I_{SERS} \propto \langle \mathbf{E}^4/\mathbf{E}_0^4 \rangle$) where $\mathbf{E}_0$ is the incident field.

The electric field enhancement and the extinction properties of metallic nanostructures are crucially dependent on the geometry and environment of the system.[13] The electric field enhancement is determined by the strength of the electric field in the particle (due to plasmonic absorption) and the scattered field due to radiative effects (which become apparent when the size of the nanostructure is a finite fraction of the incident wavelength). Because of this, the maximum field enhancement generally follows the trend of the extinction cross section ($C_{Ext} = C_{Abs} + C_{Scat}$). For example, the field enhancement on small silver nanospheres is strongly enhanced in the UV and blue part of the visible spectrum, where silver spheres absorb strongly. For gold and silver nanoparticles, shifting the LSPR to the red (by increasing the aspect ratio of a nanorod for example) increases the extinction of the particles and also increases the field enhancement.[14] Beyond this, confining the electric field to a smaller volume[15] by using substrates with small gaps (e.g., dimers of spheres[16,17]) has increased the electric field strength to the level where single molecules can be detected using SERS.[18−20]

This large enhancement of the Raman signal has enabled SERS to be used in sensing in biological fluids,[21−23] forensic analysis of drugs,[24−29] and the identification of a diverse range of analytes including chemical warfare agents,[30−32] pigments, and dyes used in works of art.[33] For many of these applications, the substrate must exhibit a number of critical and auxiliary properties. The essential properties include robustness and reproducibly high enhancement over large areas of the substrate. The primary auxiliary property is cost; substrates that require optical lithographic patterning or complex synthesis will, in general, be more costly to manufacture on large scales than those that do not.

Metal immobilized nanorod assembly (submitted) substrates may prove advantageous with respect to all of these properties. In a typical film-over-sphere substrate, silver or gold is evaporated or sputtered onto a monolayer of polystyrene or silica nano- or microspheres. Depending on the details of the metal film deposition, the film may be continuous[34] or in the case of Immobilized Nanorod Assembly (INRA) substrates contain nanoscale pillars separated by small gaps. These nanopillars are similar to those previously reported on a planar surface by Dluhy et al.[35]

Lin et al. have discussed the effect of increasing the size of the polystyrene spheres on the SERS enhancement at a fixed laser wavelength (532 nm).[36] They show that the dielectric

Special Issue: Nanostructured-Enhanced Photoenergy Conversion

Received: November 2, 2012
Revised: December 14, 2012

   dx.doi.org/10.1021/jp310846j | J. Phys. Chem. C XXXX, XXX, XXX−XXX

sphere size can be optimized to give optimum SERS intensity. Experiments such as those by Lin et al. show that it is critically important that incident laser frequency overlaps with the energy of the LSPR. Previous wavelength-scanned SERS experiments by McFarland et al. have shown that for a fixed Raman shift the surface plasmon wavelength should be halfway between the incident laser wavelength and the Stokes shifted wavelength.[37] These authors showed that the SERS enhancement factor increases as the LSPR and laser wavelength are simultaneously shifted toward the red (up to a maximum wavelength of 785 nm).

Here we investigate the enhancement factor of AgINRA substrates as a function of both the dielectric sphere diameter (310−780 nm) and the input laser wavelength (532−1064 nm). To isolate the electromagnetic enhancement from the chemical and resonance enhancements, we have chosen to use the nonresonant molecule benzenethiol as the SERS reporter. Our goal in this work is to show how INRA substrates can be optimized for applications at 1064 nm. This study will also provide insight into how the optimized SERS enhancement factor varies with wavelength in the near-IR. Although there have been past SERS measurements at 1064 nm, there have been serious questions[17] as to whether the intrinsic enhancement factor at this wavelength can be larger than at the more commonly studied wavelengths in the 600−800 nm region.

EXPERIMENTAL DETAILS

AgINRA SERS Substrate Fabrication. Glass coverslips (Fisherbrand, #1s) and polished Silicon wafers (MEMC Electronics) were used as supports for SERS substrates made as described in prior publications.[38,39] Silica (Bangs Laboratories) and polystyrene (Invitrogen) nanospheres were diluted to 5% by volume. The solvent was replaced twice with Millipore (Milli-Q, 18.2 MΩ cm^{-1}) ultrapure H_2O by a conventional centrifugation/supernatant removal procedure followed by sonication for a minimum of 1 h. An amount of 7−10 μL of solvent were drop-coated and hand-packed onto the glass or silicon support. The solvent was then allowed to evaporate in ambient conditions, at which time the nanospheres formed a close-packed array. Ag films (200-nm thick) were then deposited at a rate of 3 Å s^{-1} under high vacuum (2.0×10^{-7} Torr) over the nanosphere-covered surface using a home-built thermal vapor deposition system.[40,41] The substrates were spun at ∼550 rpm during deposition, while Ag mass thickness and deposition rate were measured by a 6 MHz gold-plated quartz crystal microbalance purchased from Sigma Instruments (Fort Collins, CO). Spinning during deposition imparts a shuttering effect to the exposed surface leading to nanopillar growth. SEM images of fabricated AgINRA substrates are presented in the inset of Figure 1.

UV−vis Diffuse Reflectance Spectroscopy. A Perkin-Elmer LAMBDA 1050 UV/vis/NIR spectrophotometer with Perkin-Elmer Integrating Sphere 150 mm UV/vis/NIR (InGaAs) Module was used for all UV−vis reflectance measurements.

Raman Spectroscopy. The Raman spectroscopy instrument used was based on an inverted microscope (Nikon Eclipse Ti). A series of diode-based lasers were used for single frequency experiments, including: (1) Spectra Physics Excelsior 1064 nm, (2) Spectra Physics HeNe, and (3) Innovative Photonics Solutions stabilized 785 nm. The detection system for 633 and 785 nm studies was an imaging spectrograph (Acton SpectraPro 2300i) with a LN_2-cooled back-thinned deep-depletion charge-coupled device (CCD) detector (Roper, model Spec 10:400BR, 1340 × 400 pixels). Additionally, the deep-depletion CCD eliminates etaloning and increases quantum efficiency for NIR studies. A second detection system was used for IR Raman studies, consisting of a spectrograph (Acton SpectraPro 2300i) configured for IR wavelengths along with a liquid N_2 cooled InGaAs array detector (Roper, model OMA V 1024−1.7, 1024 pixels). The excitation sources were brought in through the back entrance of the microscope and then focused down to a 70 μm × 70 μm spot onto the opaque AgINRA substrates using a 20× microscope objective (wd = 2.1 mm).

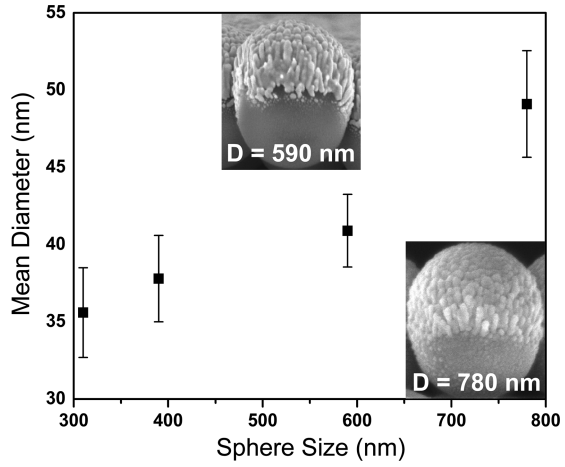

Figure 1. Plot of mean pillar diameter against sphere mask diameter on AgINRA SERS substrates. Values are an average of 20 pillars measured on a single image. SEM images (inset) are (*upper*) 75× magnification image of 200 nm Ag on 590 nm silica spheres and (*lower*) 68× magnification image of 200 nm Ag on 780 nm silica spheres. Images were recorded by Anne-Isabelle Henry at Northwestern University's Electron Probe Instrumentation Center (EPIC).

Electrodynamics Simulations. Two-dimensional finite difference time domain (FDTD) simulations were performed with the open source code "MEEP"[42] using a Drude +6 Lorentz oscillator model for the dielectric function of silver, which was a fit to the data of Johnson and Christy.[43]

RESULTS AND DISCUSSION

LSPR Spectral Location Study. Vapor deposition of silver over the support spheres produced a forest of nanopillars grown normal to the planar substrate wafer. The diameter of the pillars increased with the diameter of the sphere mask underneath. Figure 1 shows that the average pillar diameter increased from 35.6 ± 2.9 with 310 nm spheres to 49.1 ± 3.45 with 780 nm spheres. Macroscopically, the substrates appeared an iridescent dark green shifting to a brighter green color as the sphere mask diameter and LSPR wavelength increased. To determine the role of the nanopillars on the far-field scattering properties of the AgINRAs, we have compared the experimental extinction of the substrates with a two-dimensional FDTD simulation in Figure 2. The results show that the red-shift of the LSPR is correlated with increased sphere diameter due to the overall curvature of the junction between spheres, rather than because of changes in the nanoscale features of the substrate. An example simulation cell is presented in the Supporting Information.

Plasmon-Sampled Surface-Enhanced Raman Excitation Spectroscopy (PS-SERES). A fundamental enhancement

dx.doi.org/10.1021/jp310846j | J. Phys. Chem. C XXXX, XXX, XXX−XXX

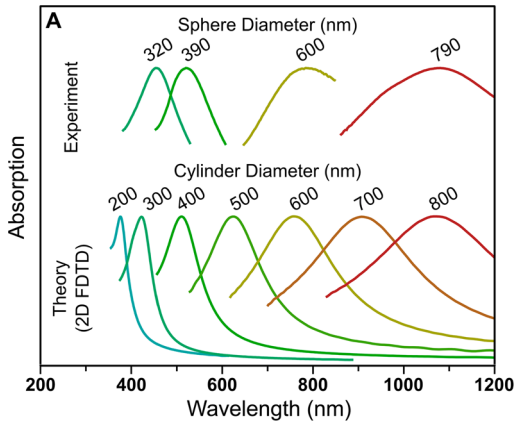

Figure 2. Normalized reflectance UV−vis spectra of AgINRA SERS substrates with diameters ranging from 320 to 790 nm (upper curves, plotted as absorption for comparison to theory). Two-dimensional FDTD simulations show that the resonance position is correlated with the sphere diameter, and the nanopillars are not required to determine the far-field scattering properties. An example simulation cell is available in the Supporting Information.

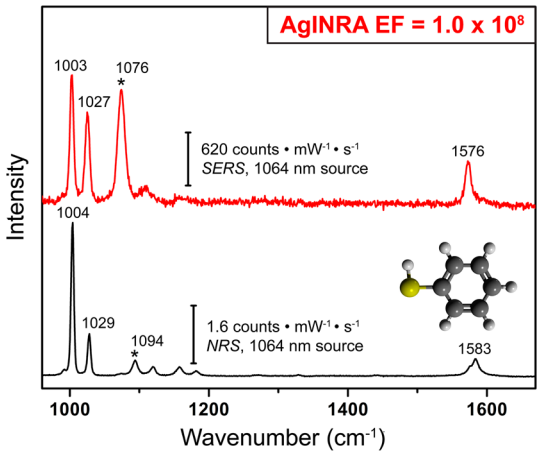

Figure 3. Comparison of neat solution normal Raman (NRS) and monolayer surface-enhanced Raman (SERS) spectra of benzenethiol on a AgINRA SERS substrate with 1064 nm CW excitation. The starred 1070 cm^{-1} peak was used for calculation of the substrate EF. The solution Raman spectrum was recorded at 299 mW with 30 s acquisition time. The SERS spectrum was recorded at 380 μW with 10 s acquisition time.

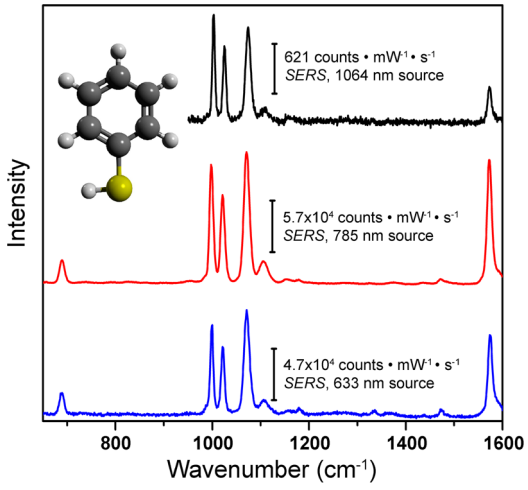

Figure 4. Comparison of monolayer SERS spectra of benzenethiol on a AgINRA SERS substrate with 633 (top), 785 (middle), and 1064 (bottom) nm CW excitation. The 1070 cm^{-1} peak was used for calculation of substrate EF as explained in eq 1. The 633, 785, and 1064 nm SERS plots were recorded at 110, 317, and 380 μW with 1.0, 0.5, and 10 s acquisition times, respectively.

factor (EF) was measured for each fabricated substrate at three different excitation wavelengths with benzenethiol as the probe molecule. Due to their common usage in the field of Raman spectroscopy, the 633, 785, and 1064 nm excitation lines were chosen. The EF is a ratio of SERS scattered photons to normal, nonenhanced Raman (RS) scattered photons of the same molecule, corrected for the number of the molecules illuminated

$$\mathrm{EF} = \frac{I_{\mathrm{SERS}}/N_{\mathrm{SERS}}}{I_{\mathrm{RS}}/N_{\mathrm{RS}}} \quad (1)$$

where I_{SERS} and I_{RS} are the Raman intensity of the 1070 cm^{-1} peak measured on the SERS substrate and in solution, respectively. N is the number of molecules excited. The surface coverage of benzenethiol was taken from the literature as 6.8×10^{14} molecules cm^{-2}.[44,45] All measured intensities were normalized for power and acquisition time and reported in units of normalized intensity (counts mW^{-1} s^{-1}). Figure 3 shows an example of SERS vs solution normal Raman spectra (NRS) used for the EF calculations at 1064 nm (see Supporting Information for a comparison of SERS and NRS at 633 and 785 nm).

For applications involving purely analytical work, the total signal is more important than the EF. To this end, we report the SERS total intensity normalized for acquisition time and incident power in Figure 4. The normalized SERS intensity measured with 633 nm excitation was ~80× higher than was measured with 1064 nm excitation, and the maximum signal was measured at 785 nm.

For this class of substrates, it has been shown[46] that the maximum enhancement of the Raman signal occurs when the LSPR providing the enhancement lies between the laser excitation wavelength and the chosen Raman-scattered photon wavelength. To optimally tune the resonance position to the SERS excitation wavelength, we measured the average EFs of each substrate at each of the three excitation wavelengths (see Figure 5). Five spots were measured at various positions on the substrate and averaged. These plasmon-sampled SERS results show peaks close to the excitation wavelength, as expected based on earlier work.[47] As the plasmon resonance is excited further to the red, the EF rises from 1.3×10^7 at 633 nm to 4.9×10^7 at 785 nm. Finally, the average EF measured with a substrate optimized for 1064 nm excitation was 1.0×10^8. This is the highest EF measured on this type of substrate to date and reflects advances made in substrate optimization as well as uniformity at the 100 μm scale relevant to CW laser Raman studies. The significant increase in EF with 1064 nm excitation occurs concurrently with a lowering of the benzenethiol molecule's Raman cross section at this excitation wavelength. The EF is a fundamental property of the SERS substrate, allowing for it to rise even though the Raman cross-section and overall signal intensity may drop.

To explain the increase in the enhancement factor as the laser wavelength approaches the infrared, we introduce a generic plasmon quality factor[14,48] $Q_{\mathrm{SPP}} = \varepsilon_r^2/\varepsilon_i$ where ε_r and ε_i are the real and imaginary parts of the frequency-dependent

dx.doi.org/10.1021/jp310846j | J. Phys. Chem. C XXXX, XXX, XXX−XXX

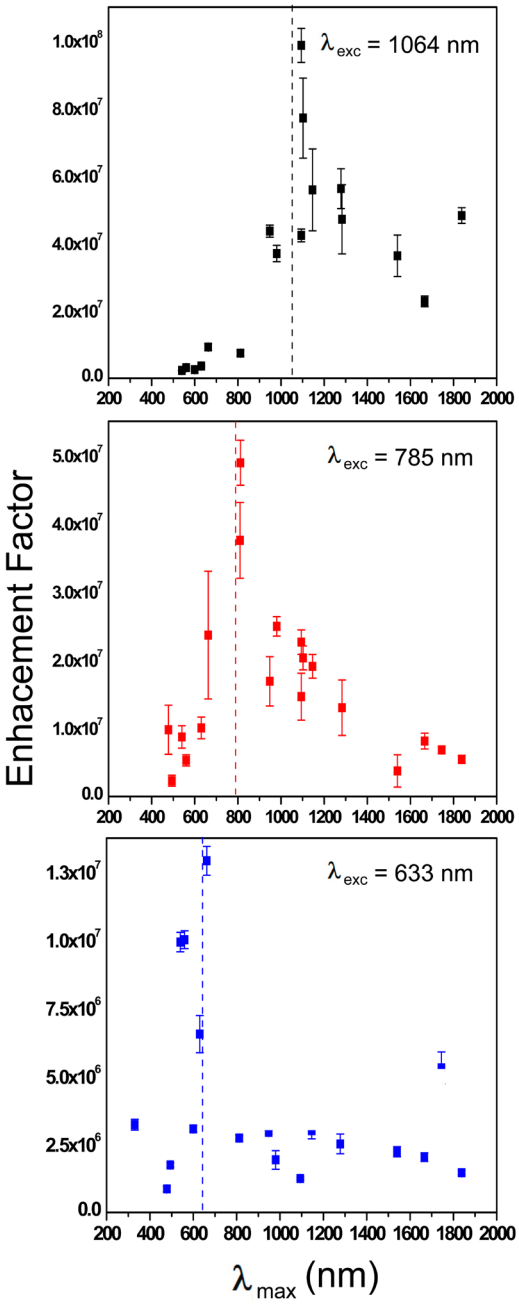

Figure 5. Plot of five-spot averages of fundamental enhancement factor (EF) measured on AgINRA SERS substrates with varying sphere size and LSPR maxima (λ_{max}). Vertical lines are included for guidance and correspond with 633 nm (blue), 785 nm (red), and 1064 nm (black) excitation wavelengths.

dielectric function of silver. Q_{SPP} describes the level of field confinement in surface plasmon polariton systems and also in particulate systems where anisotropy allows for plasmon-induced charges on the nanoparticle to be spatially separated (for example, nanorods). In the EM mechanism for SERS, the enhancement factor is related to the fourth power of the electric field ($\mathbf{E}^4$), which is proportional to Q_{SPP}^2 when the system is on resonance. The proportionality between the EF and Q_{SPP}^2 depends on a geometry-dependent prefactor α, giving EF = $\alpha \cdot Q_{SPP}^2$. For the INRA substrates, we determined α via an empirical fit to be approximately 10.5. Figure 6 shows that the quality factor is in excellent agreement with the

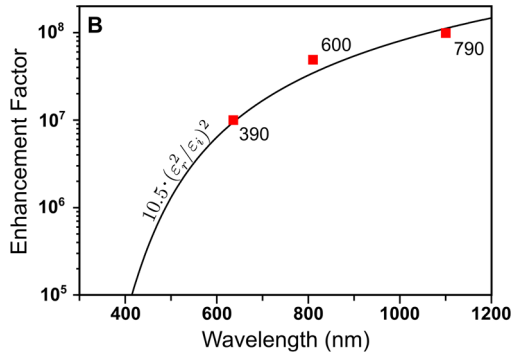

Figure 6. Enhancement factors for the three AgINRA SERS substrates that performed optimally at the laser wavelengths of 633, 785, and 1064 nm (dquares). The enhancement factor scales like Q_{SPP}^2, where Q_{SPP} qualitatively describes the amount of electromagnetic field confinement (black curve, see text). There is a geometric prefactor of 10.5 that is an empirical fit to the data.

measured enhancement factors at the three wavelengths considered. Overall, the metric describes the relative scaling of the field strength and predicts that the field enhancement will increase 1.5 orders of magnitude between 633 and 1064 nm, assuming that the system is optimized for resonances at these excitation wavelengths. Further, the comparison suggests that the enhancement factor will continue to rise at even longer wavelengths than are considered here.

CONCLUSIONS

SERS substrates were fabricated and optimized across the visible spectrum and into the near-infrared region using PS-SERES. Optimization of the silver Immobilized Nanorod Assembly (AgINRA) substrates was accomplished by utilizing the plasmonic properties of metal nanopillars on the surface to tune an excitable optical resonance in the metal. In this study, metal film thickness was held constant, while the diameters of the spheres in the mask underneath were varied. The correlation between support sphere size and LSPR agrees with theory as presented and follows the predicted trend of red-shifting with wider sphere diameters. Higher enhancement factors (EFs) were measured as the INRA's LSPR was moved toward the infrared region and its relative positioning with respect to excitation wavelength was optimized, leading to increased photon−plasmon coupling and strong localization of electromagnetic energy in nanometer scale crevices on the surface. This result provides more evidence to suggest that the electromagnetic mechanism is the overwhelmingly dominant contributor to the SERS enhancement effect. An EF of 1.0×10^8 was measured for excitation at 1064 nm and a plasmon resonance ~1100 nm. This is the highest EF to date measured on this type of large-area SERS substrate. Coupled with their robustness and ease of fabrication, these results further underscore the value and versatility of metal INRA substrates in the field of surface-enhanced Raman spectroscopy, and they demonstrate that higher enhancement factors are possible at 1064 nm than at shorter wavelengths.

ASSOCIATED CONTENT

Supporting Information

An example unit cell used in the two-dimensional FDTD simulations and a demonstration of the photon−plasmon spectral relationship are included, along with more representa-

dx.doi.org/10.1021/jp310846j | J. Phys. Chem. C XXXX, XXX, XXX−XXX

tive Raman spectra. This material is available free of charge via the Internet at http://pubs.acs.org.

AUTHOR INFORMATION

Corresponding Author

*E-mail: vanduyne@northwestern.edu.

Notes

The authors declare no competing financial interest.

ACKNOWLEDGMENTS

This work was supported by the National Science Foundation (DMR-1121262) and by the Defense Advanced Research Projects Agency (N66001-11-1-4179 and FA9550-08-1-0221). Also, much appreciation is extended to Matthew Sonntag for contributing Matlab scripts for the experimental data analysis.

REFERENCES

(1) Efrima, S.; Metiu, H. *J. Chem. Phys.* **1979**, *70*, 1602−1613.
(2) Gersten, J.; Nitzan, A. *J. Chem. Phys.* **1980**, *73*, 3023−3037.
(3) Kerker, M.; Wang, D. S.; Chew, H. *Appl. Opt.* **1980**, *19*, 4159−4174.
(4) Xu, H. X.; Kall, M. Estimating SERS properties of silver-particle aggregates through generalized Mie theory. In *Surface-Enhanced Raman Scattering: Physics and Applications*; Springer-Verlag: Berlin, 2006; *Vol. 103*, pp 87−103.
(5) Weitz, D. A.; Garoff, S.; Gersten, J. I.; Nitzan, A. *J. Chem. Phys.* **1983**, *78*, 5324−5338.
(6) Achermann, M. *J. Phys. Chem. Lett.* **2010**, *1*, 2837−2843.
(7) Standridge, S. D.; Schatz, G. C.; Hupp, J. T. *J. Am. Chem. Soc.* **2009**, *131*, 8407−8409.
(8) Fleischmann, M.; Hendra, P. J.; McQuillan, A. J. *Chem. Phys. Lett.* **1974**, *26*, 163−166.
(9) Jeanmaire, D. L.; Van Duyne, R. P. *J. Electroanal. Chem. Interfacial Electrochem.* **1977**, *84*, 1−20.
(10) Garcia-Vidal, F. J.; Pendry, J. B. *Phys. Rev. Lett.* **1996**, *77*, 1163−1166.
(11) Le Ru, E. C.; Blackie, E.; Meyer, M.; Etchegoin, P. G. *J. Phys. Chem. C* **2007**, *111*, 13794−13803.
(12) Morton, S. M.; Jensen, L. *J. Am. Chem. Soc.* **2009**, *131*, 4090−4098.
(13) Kelly, K. L.; Coronado, E.; Zhao, L. L.; Schatz, G. C. *J. Phys. Chem. B* **2003**, *107*, 668−677.
(14) Arnold, M. D.; Blaber, M. G. *Opt. Express* **2009**, *17*, 3835−3847.
(15) Maier, S. A. *Opt. Express* **2006**, *14*, 1957−1964.
(16) Wustholz, K. L.; Henry, A.-I.; McMahon, J. M.; Freeman, R. G.; Valley, N.; Piotti, M. E.; Natan, M. J.; Schatz, G. C.; Van Duyne, R. P. *J. Am. Chem. Soc.* **2010**, *132*, 10903−10910.
(17) Blaber, M. G.; Schatz, G. C. *Chem. Commun.* **2011**, *47*, 3769−3771.
(18) Nie, S.; Emory, S. R. *Science* **1997**, *275*, 1102−1106.
(19) Kleinman, S. L.; Ringe, E.; Valley, N.; Wustholz, K. L.; Phillips, E.; Scheidt, K. A.; Schatz, G. C.; Van Duyne, R. P. *J. Am. Chem. Soc.* **2011**, *133*, 4115−4122.
(20) Sonntag, M. D.; Klingsporn, J. M.; Garibay, L. K.; Roberts, J. M.; Dieringer, J. A.; Seideman, T.; Scheidt, K. A.; Jensen, L.; Schatz, G. C.; Van Duyne, R. P. *J. Phys. Chem. C* **2012**, *116*, 478−483.
(21) Shafer-Peltier, K. E.; Haynes, C. L.; Glucksberg, M. R.; Van Duyne, R. P. *J. Am. Chem. Soc.* **2003**, *125*, 588−593.
(22) Anker, J. N.; Hall, W. P.; Lyandres, O.; Shah, N. C.; Zhao, J.; Van Duyne, R. P. *Nat. Mater.* **2008**, *7*, 442−453.
(23) Zhao, J.; Zhang, X.; Yonzon, C. R.; Haes, A. J.; Van Duyne, R. P. *Nanomedicine (London, U. K.)* **2006**, *1*, 219−228.
(24) Das, A.; Zhao, J.; Schatz, G. C.; Sligar, S. G.; Van Duyne, R. P. *Anal. Chem.* **2009**, *81*, 3754−3759.
(25) Canamares, M. V.; Lombardi, J. R.; Leona, M. *J. Raman Spectrosc.* **2008**, *39*, 1907−1914.
(26) Carter, J. C.; Brewer, W. E.; Angel, S. M. *Appl. Spectrosc.* **2000**, *54*, 1876−1881.
(27) Chen, J. W.; Jiang, J. H.; Gao, X.; Liu, G. K.; Shen, G. L.; Yu, R. Q. *Chem.−Eur. J* **2008**, *14*, 8374−8382.
(28) Farquharson, S.; Inscore, F. E.; Gift, A. D.; Shende, C. S. SERS method for rapid pharmacokinetic analysis of drugs in saliva. U.S. Patent 7393692, Jul 1, 2008
(29) Sulk, R. A.; Corcoran, R. C.; Carron, K. T. *Appl. Spectrosc.* **1999**, *53*, 954−959.
(30) Pearman, W. F.; Fountain, A. W. *Appl. Spectrosc.* **2006**, *60*, 356−365.
(31) Biggs, K. B.; Camden, J. P.; Anker, J. N.; Van Duyne, R. P. *J. Phys. Chem. A* **2009**, *113*, 4581−4586.
(32) Zhang, X.; Van Duyne, R. P. *Mater. Res. Soc. Symp. Proc.* **2005**, *876E*, R8−54.
(33) Wustholz, K. L.; Brosseau, C. L.; Casadio, F.; Van Duyne, R. P. *Phys. Chem. Chem. Phys.* **2009**, *11*, 7350−7359.
(34) Farcau, C.; Astilean, S. *J. Phys. Chem. C* **2010**, *114*, 11717−11722.
(35) Chu, H. Y.; Liu, Y. J.; Huang, Y. W.; Zhao, Y. P. *Opt. Express* **2007**, *15*, 12230−12239.
(36) Lin, W.-C.; Liao, L.-S.; Chen, Y.-H.; Chang, H.-C.; Tsai, D.; Chiang, H.-P. *Plasmonics* **2011**, *6*, 201−206.
(37) McFarland, A. D.; Young, M. A.; Dieringer, J. A.; Van Duyne, R. P. *J. Phys. Chem. B* **2005**, *109*, 11279−11285.
(38) Dick, L. A.; McFarland, A. D.; Haynes, C. L.; Van Duyne, R. P. *J. Phys. Chem. B* **2002**, *106*, 853−860.
(39) Litorja, M.; Haynes, C. L.; Haes, A. J.; Jensen, T. R.; Van Duyne, R. P. *J. Phys. Chem. B* **2001**, *105*, 6907−6915.
(40) Haynes, C. L.; Haes, A. J.; Van Duyne, R. P. *Mater. Res. Soc. Symp. Proc.* **2001**, *635*, C6.3/1−C6.3/6.
(41) Stiles, P. L.; Dieringer, J. A.; Shah, N. C.; Van Duyne, R. P. *Annu. Rev. Anal. Chem.* **2008**, *1*, 601−626.
(42) Oskooi, A. F.; Roundy, D.; Ibanescu, M.; Bermel, P.; Joannopoulos, J. D.; Johnson, S. G. *Comput. Phys. Commun.* **2010**, *181*, 687−702.
(43) Johnson, P. B.; Christy, R. W. *Phys. Rev. B* **1972**, *6*, 4370.
(44) Wan, L.-J.; Terashima, M.; Noda, H.; Osawa, M. *J. Phys. Chem. B* **2000**, *104*, 3563−3569.
(45) Whelan, C. M.; Smyth, M. R.; Barnes, C. J. *Langmuir* **1999**, *15*, 116−126.
(46) Schatz, G. C.; Young, M. A.; Van Duyne, R. P. Electromagnetic mechanism of SERS. In *Surface-Enhanced Raman Scattering: Physics and Applications*; Springer-Verlag: Berlin, 2006; Vol. *103*, pp 19−45.
(47) Haynes, C. L.; Van Duyne, R. P. *J. Phys. Chem. B* **2003**, *107*, 7426−7433.
(48) Schmucker, A. L.; Harris, N.; Banholzer, M. J.; Blaber, M. G.; Osberg, K. D.; Schatz, G. C.; Mirkin, C. A. *ACS Nano* **2010**, *4*, 5453−5463.